Sulfone-functionalized Stable Molecular Single Crystals for Photocatalytic Hydrogen Evolution

Xunliang Hu[1], Xiaoju Yang[1], Bingyi Song[1], Zhen Zhan[1,2], Ruixue Sun[1], Yantong Guo[1], Li-Ming Yang[1], Xuan Yang[1], Chun Zhang[3], Irshad Hussain[4], Xiaoyan Wang[1]*, Bien Tan[1]*

1. Key Laboratory of Material Chemistry for Energy Conversion and Storage Ministry of Education, Hubei Key Laboratory of Material Chemistry and Service Failure, School of Chemistry and Chemical Engineering, Huazhong University of Science and Technology, Luoyu Road No. 1037, 430074, Wuhan, China;

2. Department of Applied Physics, The Hong Kong Polytechnic University, Hung Hom, Kowloon, 999077, Hong Kong, China;

3. College of Life Science & Technology Huazhong University of Science and Technology Luoyu Road No. 1037,430074, Wuhan, China;

4. Department of Chemistry and Chemical Engineering, SBA School of Science and Engineering (SSE) Lahore University of Management Sciences (LUMS), Lahore Cantt, 54792, Pakistan.

ABSTRACT: Highly crystalline, hydrophilic and visible-light responsible molecular semiconductor materials are promising photocatalysts for water splitting to produce green hydrogen. However, hydrophobic nature, instability, high cost and the tedious synthesis process of most of the reported organic photocatalysts limit their photocatalytic activity and hinder their scalable applications. Herein, we report stable and easy-to-synthesize sulfone-functionalized molecular single crystals (**FSOCA**) as efficient hydrophilic photocatalyst for hydrogen evolution reaction. Its structure was determined by 3D electron diffraction technique with atomic resolution. The introduction of the sulfone groups favors the decrease of exciton binding energy, resulting in better exciton separation ability. FSOCA is highly hydrophilic in nature enabling it to efficiently drive sacrificial hydrogen evolution (760 μmol h^{-1}; 76 mmol g^{-1} h^{-1}). Interestingly, FSOCA remains stable in photocatalytic process for at least 400 hours showing negligible structure change, has and can cumulatively produce 179.2 mmol (about 4 L) of hydrogen. Employing transient spectroscopy, we find that the highly coplanar structure greatly enhances the transport of charge carriers to hole scavengers. In-situ Fourier transform infrared spectroscopy and DFT calculation shows that hydrogen bonding between sacrificial agent (ascorbic acid) with sulfone group is energetically favorable for the adsorption of ascorbic acid on FSOCA, thereby significantly improving the oxidation reaction kinetics and the photocatalytic performance. This work provides a scalable, efficient and low-cost strategy to synthesize highly active and stable organic photocatalysts, which can potentially be applicable in scalable photocatalysis.

INTRODUCTION

Direct photocatalytic water splitting via solar light to produce hydrogen as a clean fuel is regarded as ideal technology [1,2]. Organic photocatalysts are comprised of earth-abundant elements (like carbon and nitrogen), and their structure can be synthetically tuned to absorb visible light while simultaneously retaining suitable energy levels to drive a range of photocatalytic reactions [3–5]. Many organic semiconductors, especially polymeric materials, have been widely developed for photocatalytic hydrogen evolution reaction (HER), such as g-C_3N_4 [1,6], linear conjugated polymers (LCPs) [7,8], conjugated microporous polymers (CMPs) [9–11], covalent organic frameworks (COFs) [12–14] and covalent triazine-based frameworks (CTFs) [15–18]. Among polymeric materials, the state-of-the-art photocatalyst can achieve the highest HER performance of about 100 mmol g^{-1} h^{-1} [4,19], while most of these polymeric materials are difficult to synthesize and require costly monomers. Moreover, the most of polymeric materials are amorphous or semicrystalline structure with abundant defects and prone to the recombination of excitons [16,20–23]. Therefore, the synthesis of low cost and highly crystalline organic photocatalysts that are highly efficient under visible light with minimal recombination sites is highly desirable.

Organic molecular semiconductors are very appealing materials for photocatalytic applications. Diverse synthetic and processable methodologies make them feasible to tune their chemical or device structure. Moreover, it is generally easy to obtain highly crystalline and ordered structure that can efficiently facilitate the exciton diffusion [23,24]. However, till now, only handful molecular semiconductors such as photovoltaic molecules [25] (e.g., Y6's derivatives), perylenediimide [26–29], porphyrin [30–32], carbazole [33,34] are reported for photocatalytic HER. Stupp's group has carried out groundbreaking research on perylenediimide-based self-assembled supramolecular materials i.e., self-assembling hydrogel, which showed the photocatalytic HER performance of only 6.56 μL h^{-1} [26]. To the best of our knowledge, molecular materials mentioned above still suffer from the drawbacks of relatively low performance, poor stability and high cost. Most of perylenediimide, porphyrin and Y6 derivatives show low performance [25-32, 35],

for example the real activity of Y6CO is only 15 μmol h^{-1} [35]. Recently, Zhu *et al.* developed a hydrophilic perylenetetracarboxylic acid nanosheets based photocatalyst, which showed a high HER activity of 118.9 mmol g^{-1} h^{-1}, but this experiment was carried out under a very strong light source with intensity of 530 mW cm^{-2}, which is about two times stronger than that used in the common reports [3], and can directly influence the HER performance. Photocatalyst stability is also highly desired and is essential in future scalable applications. However, there is still no long-term (more than 100 hours) stability test for HER by molecular materials, which may be because of their relativity low photocatalytic stability. For instance, Cooper *et al.* observed a gradual and simultaneous decrease of crystallinity and activity for pyrene based TBAP photocatalyst in just 6 hours [23]. The high cost is another barrier that limits the development of molecular photocatalysts, for example, the synthesis procedures of carbazole [34] and Y6's [35] derivatives are too complicated and expensive. In summary, although there is some progress in molecular photocatalysis for HER, there is still a plenty of room for improvement, especially in terms of activity, stability and low-cost synthesis. More importantly, there is still a lack of a general and scalable strategy for the design and synthesis of highly crystalline, low-cost, stable and highly active molecular photocatalysts.

Recently, LCPs [36], CMPs [19] and COFs [12] containing Benzothiophene sulfone groups have shown excellent performance in photocatalytic hydrogen production for the special merits of sulfone unit, which show good interaction with water molecule and acts as the electron transfer site out of the polymer. Inspired by these, herein, a sulfone functionalized single crystal of benzo[1,2-b:4,5-b']bis[1]benzothiophene-3,9-dicarboxylic acid, 5,5,11,11-tetraoxide (**FSOCA**) was developed as photocatalyst for HER. The rigid and planar aromatic structure significantly enhance the delocalized range and the interlayer π-π interaction. Strong π-π interactions assist hydrogen bonding between carboxyl groups making it easier to get highly crystalline and stable structure. The resulting FSOCA shows a highly crystalline structure with good hydrophilicity and low exciton binding energy. FSOCA molecular crystal showed enhanced photocatalytic HER activity up to 76 mmol g^{-1} h^{-1}. Which is far higher than structurally related carboxylic acids, including [p-Terphenyl]-4,4''-dicarboxylic acid (**TPCA**), and 5,5-dioxo-5H-dibenzo[b,d]thiophene-3,7-dicarboxylic acid (**SOCA**). More importantly, FSOCA is easy to synthesize at the scale of tens of grams with high crystallinity, and remain stable even in long-term photocatalysis process (400 hours). High HER performance, good stability and easy-to-synthesize attributes of FSOCA affirm a great potential for their large-scale applications for HER.

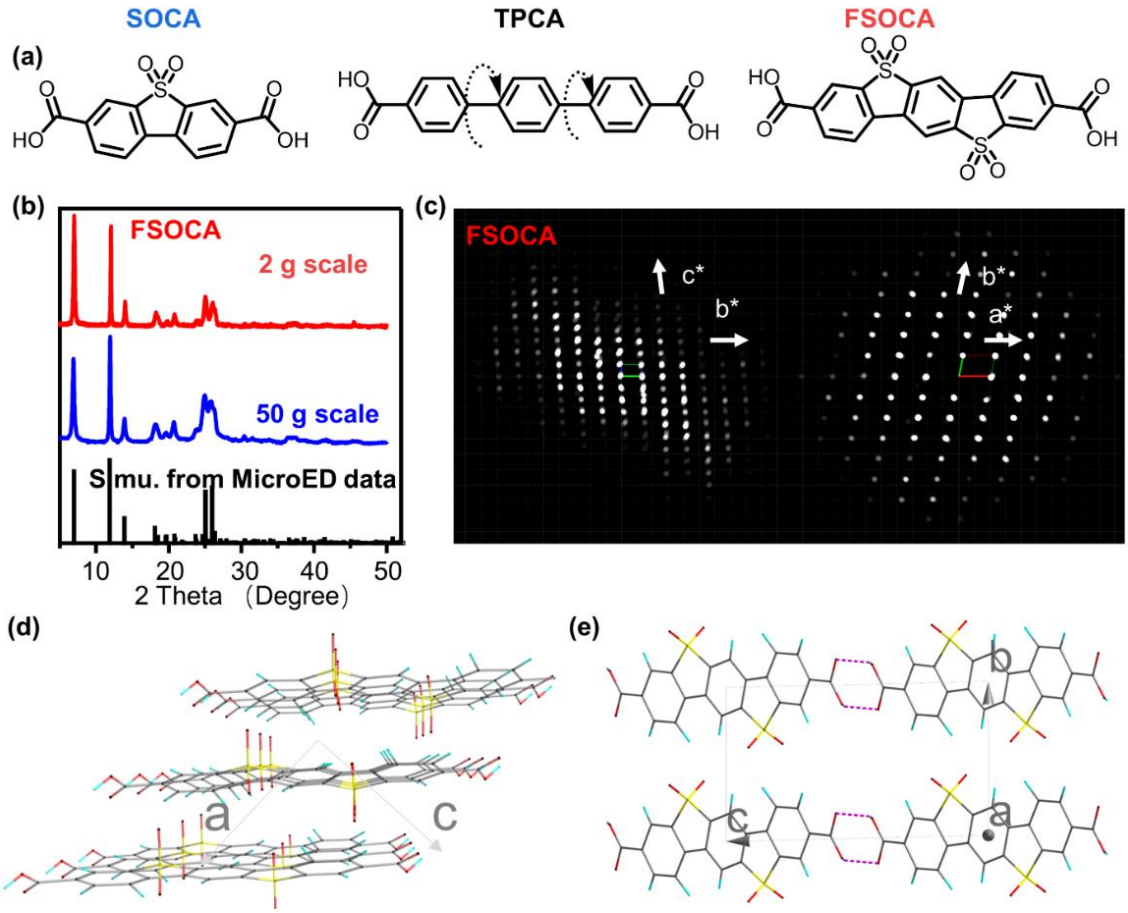

Figure 1. (a) Molecule structures of three aromatic carboxylic acid; (b) Experimental PXRD data for FSOCA from different synthesis scales and simulated PXRD data based on the crystal structure solved via cryo-electron diffraction tomography; (c) EDT data projected along the [100], [001] direction for the FSOCA with routine holder and with cryo-holder. (d) supercell structure of FSOCA view via b axis; (e) supercell structure of FSOCA view via a axis.

Results and discussion

FSOCA was synthesized via sulfonation reaction of TPCA on tens of gram-scale (Fig. 1b, Supplementary materials, synthetic procedures and Supplementary table 1 - 2). FSOCA is insoluble in most of common organic solvents and water, and slightly soluble in DMSO, while moderately soluble in N-methylpyrrolidone (NMP), an alkaline organic solvent. The ^{1}H NMR spectrum of FSOCA showed three types of chemical environments of hydrogen at 8.94 ppm, 8.31 ppm and 8.23 ppm (Supplementary Fig. 1). Additionally, as shown in Fourier transform infrared (FT-IR) spectrum (Supplementary Fig. 5), a strong peak at about 1700 cm^{-1} can be assigned to the carbonyl group (–C=O), and peaks at 2500 ~ 3100 cm^{-1} can be assigned to the carboxyl group in hydrogen bond mode (–COO···H···O=C(OH)–). To gain more structural information, large crystals (FSOCA·NMP) were obtained from NMP solution, and its structure was determined by single-crystal X-ray crystallography (SCXRD, Supplementary Fig. 3) and powder X-ray diffraction (Supplementary Fig. 9).

The control molecule TPCA was synthesized by a reported method (Supplementary materials, synthetic procedures), and its structure was confirmed by ^{1}HNMR (Supplementary Fig. 2) and FTIR (Supplementary Fig. 7). The control molecule SOCA is commercially available and can be easily crystallized in a variety of solvents. To confirm its structure, large crystals (SOCA·DMF) were obtained from DMF solution, and its structure was also confirmed via SCXRD (Supplementary Fig. 4). TGA curves showed that there was no significant weight loss below 300 ℃, and SOCA and FSOCA showed much better thermal stability than that of TPCA, which may be because of their rigid structure (Supplementary Fig. 8).

Crystal structure of FSOCA and SOCA.

After confirming the chemical structure of these carboxyl acids, we explored the crystal structures of these acid in their condensed state. Firstly, PXRD patterns show that FSOCA (Fig. 1b) and SOCA (Supplementary Fig. 10) are easily crystallized. However, there is no long-range ordered structure in TPCA (Supplementary Fig. 11), only three peaks in PXRD, which are likely originating from self-assembly structure. Then, their morphology was also observed by Scanning Electron Microscope (SEM) and Transmission Electron Microscope (TEM). FSOCA tends to form the rod-shaped, layered structure (Supplementary Fig. 12-13), and the length of rods ranges from 500 nm to tens of micrometers. SOCA is also nanorod-type structure with about 20 μm long rods (Supplementary Fig. 14). TPCA, however, is in the form of irregular nanosheet (Supplementary Fig. 15). Interestingly, FSOCA's morphology was solvent-dependent (Supplementary Fig. 16-18), possibly due to the exfoliation of the layered structure in organic solvents followed by the reassembling process. The Atomic Force Microscope (AFM) images of FSOCA in acetone showed nanosheets-like morphology with thickness of about 4 nm, while it shows nanorod-like structure in water with size about 100 nm (Supplementary Fig. 19).

Crystal size of FSOCA and SOCA was too small to investigate their structure via SCXRD, so microcrystal electron diffraction (MicroED) was used to analyse their structure. The lattice constants of FSOCA (Fig. 1c-1e) were determined to be a = 5.06 Å, b = 7.63 Å, c = 12.97 Å, α = 89.07°, β = 100.93°, γ = 101.94°, V = 480.9 $Å^3$ from the reconstructed 3D lattice in reciprocal space. Crystal structure of FSOCA was found to belong to the space group $P\bar{1}$ (No.2). Fig. 1d-1e are stacking model of FSOCA along different axes. In a unit cell, FSOCA molecules were connected via the hydrogen bonding between carboxylic acid group (Fig. 1e), the distance between the two oxygen atoms is 2.64 Å, which is consistent with the typical hydrogen bond length. Then, one-dimensional carboxylic acid chains are connected via hydrogen bonding are further stacked together via the π-π interaction to form the 3D structure (Fig. 1d and Supplementary Fig. 20). Lattice constants of SOCA were determined to be a = 19.27 Å, b = 14.31 Å, c = 5.03 Å, α = 90.00°, β = 92.48°, γ = 90.00°, V = 1385.7 $Å^3$ (Supplementary Fig. 21). The crystal structure of SOCA was found to belong to the space group $P2_1$ (No.4). In a unit cell (Supplementary Fig. 22), nine SOCA molecules were connected via the hydrogen bond of two carboxyl group. Then 3d crystals were constructed via the stack of one-dimensional carboxylic acid chains (Supplementary Fig. 22 - 23).

Photoelectrochemical characterization

The introduction of sulfone groups was expected to enhance the hydrophilicity of developed organic photocatalysts that was confirmed by contact angle measurement. Water contact angles (Fig. 2a-2c) show that both FSOCA and SOCA are hydrophilic (the water contact is about 36~39°), while TPCA is relatively hydrophobic (the water contact angle is 92°) in nature. Dynamic light scattering (Supplementary Fig. 24) shows relative narrow distribution size of SOCA (the peak: 460~610nm) and FSOCA (the peak: 450~600nm) in water, while TPCA shows a broad size distribution (the peak: 710~1280nm). These results confirmed that both SOCA and FSOCA possess much better hydrophilicity and dispersibility in water than that of TPCA. Eb has been regarded as a crucial parameter for mediating charge separation in organic photocatalysts. Minimizing the Eb of organic photocatalyst can increase the yield of charge-carrier generation and thus improve the photocatalytic activities. So, the Eb of these compounds were estimated from the temperature-dependent photoluminescence (PL) spectra (Fig. 2d-f). Upon a decrease in temperature, the integrated PL peak intensity increased gradually, and the corresponding Eb was calculated by fitting these data using the Arrhenius equation, $I(T) = I_0 / (1 + A \exp(-Eb/ k_B \times T))$. Accordingly, the Eb of FSOCA, SOCA and TPCA was calculated to be 44 meV, 14 meV and 210 meV, respectively. These results confirm that locking the benzene ring by the sulfone group can effectively reduce the exciton binding energy. The smaller Eb of FSOCA and SOCA means the weaker interaction of electron–hole pairs, while the excitons are much easier separated as carries[34].

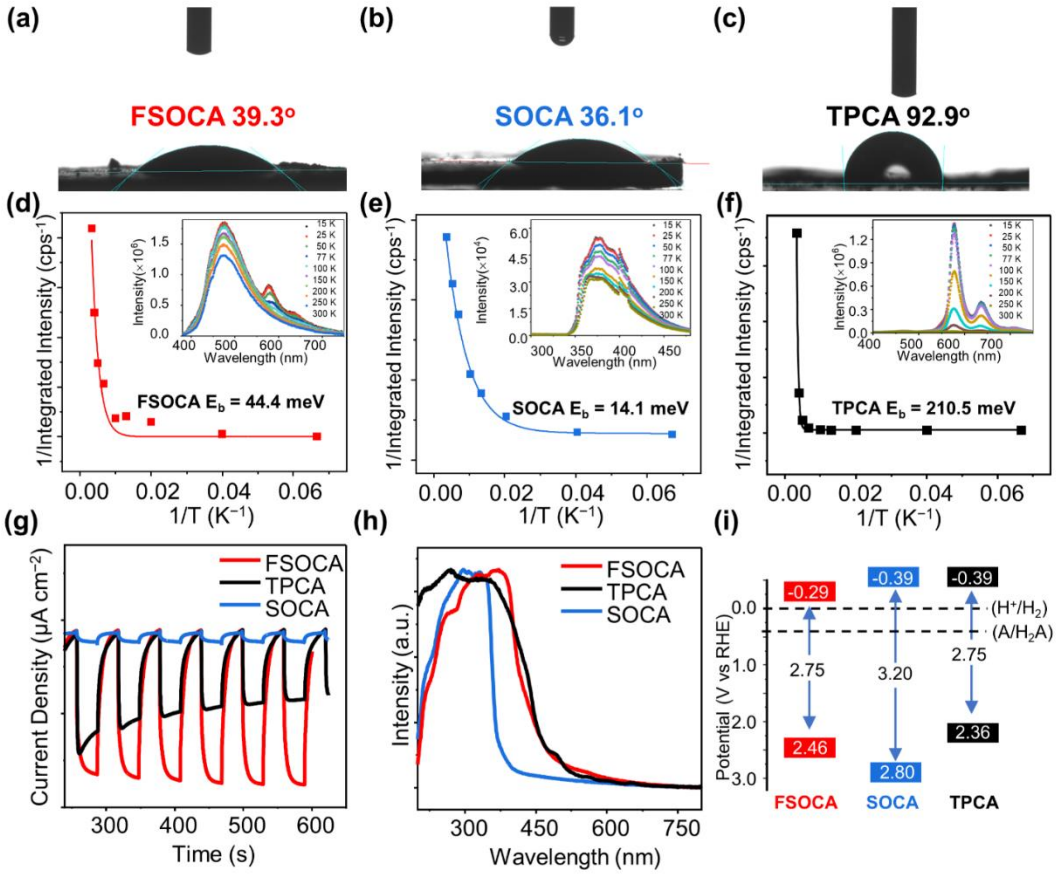

Figure 2. Water contact angle of (a) FSOCA. (b) SOCA. (c) TPCA. (d-f) The integrated PL emission intensity as a function of temperature of FSOCA, SOCA and TPCA in solid state. (g) The photocurrent curves. (h) The UV–vis absorption spectra for FSOCA, SOCA and TPCA. (h) The energy level of FSOCA, SOCA and TPCA.

Next, we explored photoelectric properties of three developed organic photocatalysts by spectroscopic analysis. UV–vis reflectance spectra of these photocatalysts were measured in the solid state, and the absorption onset was found to be about 370 nm (SOCA), 450 nm (FSOCA) and 460 nm (TPCA) (Fig. 2h). Photoelectrochemical measurements provide evidence for the modulation of charge mobility in these photocatalysts (Fig. 2g). The photocurrent displays stable photogenerated charges reaching the surface of FSOCA. However, the photocurrent of TPCA decreased significantly with time, and SOCA showed very low photocurrent which may be because of its limited absorption in UV-Vis light range. Steady state fluorescence spectra of FSOCA, SOCA and TPCA in solid state (298 K) showed the maximum emission wavelength of at 478 nm, 380 nm and 572 nm, respectively. The corresponded average lifetime was calculated as 2.08 ns, 0.56 ns and 6.68 ns for FSOCA, SOCA and TPCA, respectively (Supplementary Fig. 25). The conduction band (CB) and valence band (VB) positions of three developed photocatalysts were estimated by electrochemical Mott–Schottky plots and their optical band gaps were found suitable for both proton reduction and water oxidation reaction (Fig. 2i and Supplementary Fig. 1). The positive slope of Mott–Schottky plots indicates a typical n-type semiconductor feature. The VB and CB energy of FSOCA was slightly lower than TPCA, which may be due to the electron withdrawing nature of the sulfone groups.

Photocatalytic experiment

Better wettability and low exciton binding energy indicated that these organic photocatalysts could possess good photocatalytic ability. Therefore, we set out to explore their utilization as light-absorbing units to photocatalytic water reduction using ascorbic acid (AA) as a sacrificial electron donor (SED) and Pt as a co-catalyst. All materials evolved hydrogen under UV-Vis light ($\lambda > 320$ nm, 250 mW cm^{-2}, Fig. 3a) and the average HERs were determined to be 570 μmol h^{-1} (57 mmol g^{-1} h^{-1}) for FSOCA (Supplementary Fig. 2). When the photon flux was ~330 mW cm^{-2} provided by Xe light of $\lambda \geq 320$ nm, the performance of FSOCA can be as high as 760 μmol h^{-1} (76 mmol g^{-1} h^{-1}). This is almost one of the best organic photocatalysts reported thus far, and its photocatalytic activity is comparable with most of metal-containing inorganic photocatalysts (Supplementary table 4).

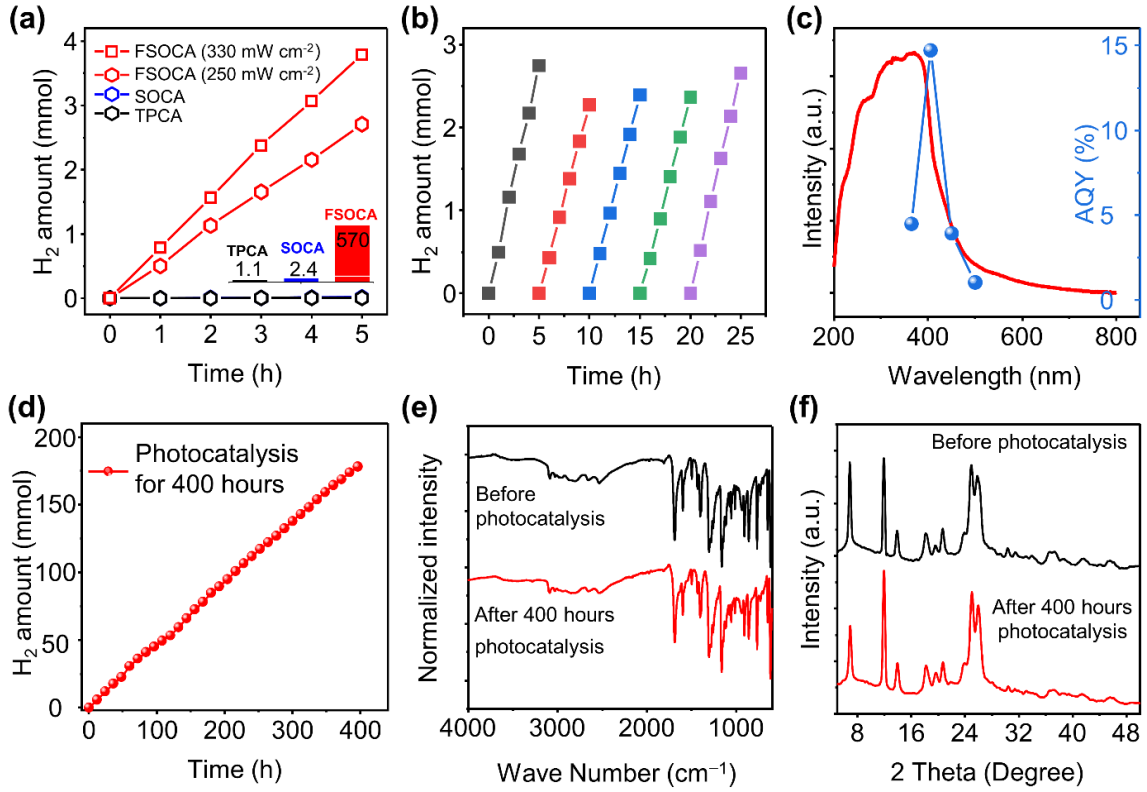

Figure 3. (a) Photocatalytic HER under full spectrum (λ ≥ 320 nm) of FSOCA, SOCA and TPCA (the inset is the performance comparison of TPCA, SOCA and FSOCA, the units are μmol h^{-1}). (b) The cycle photocatalytic HER performance of FSOCA under full spectrum. Reaction conditions: 10.0 mg photocatalyst, 1.0 wt% Pt as a cocatalyst, 100 mL of a 1.0 M ascorbic acid solution, pH 2.4. (c) The wavelength-dependent AQY for photocatalytic HER over FSOCA. (d) The accumulated H_2 amount in a long term (400 h) photocatalytic experiment of FSOCA (10.0 mg photocatalyst, 1.0 wt% Pt as a cocatalyst, λ ≥ 320 nm, light intensity: ~250 mW cm^{-2}). (e) The FTIR spectra of FSOCA before and after 400 hours of photocatalysis experiment. (f) The PXRD pattern of FSOCA before and after 400 hours of photocatalysis experiment.

The H_2 evolution of the original TPCA was only 1/500 of FSOCA (1.1 μmol h^{-1}; 110 μmol g^{-1} h^{-1}), which highlights a significant influence of the sulfone groups on the molecular photocatalytic performance. Otherwise, H_2 evolution of the SOCA was also very low (2.4 μmol h^{-1}; 240 μmol g^{-1} h^{-1}), which may be due to the limited light absorption (Supplementary Fig. 3). Furthermore, the optimized Pt loading amount for FSOCA was about 0.43 wt%, as tested by ICP-MS (Supplementary Fig. 29, Supplementary table 5). FSOCA could retain its HER activity to over five cycles (Fig. 3b), and continuous hydrogen production over 24 h (Supplementary Fig. 30) without a significant decrease in its activity displaying its good stability. The apparent quantum yield (AQY) was measured at different light wavelengths by monochromatic light (Supplementary Table 3). The AQY value at 405 nm (±10 nm) was calculated to be 14.7% (Fig. 3c).

Long term photocatalytic experiments (400 h) were conducted to verify the performance and structural stability of FSOCA (Fig. 3d-3f, Supplementary Fig. 31). FSOCA exhibits continuous hydrogen evolution without significant attenuation in the photocatalytic activity during the cycling photocatalytic experiment lasting for 400 hours (Fig. 3d and Supplementary Fig. 31). Furthermore, FSOCA retained its chemical structure, crystalline structure and morphology of after recycling (Fig. 3e-3f, and Supplementary Figs. 32-33). The FTIR (Fig. 3e) and PXRD pattern (Fig. 3f) of FSOCA are similar before and after 400 hours of photocatalysis experiment, which confirms that its structure remains intact in the photocatalytic process. The TEM images of FSOCA after photocatalysis experiment show abundant Pt nanoparticles (size from 2.0 nm to 5.0 nm) on the edges and surface of FSOCA (Supplementary Fig. 33).

Transient spectroscopy.

As light absorption and charge separation process are the key initial steps to photocatalysis, we used ultrafast transient absorption spectroscopy (uf-TAS) to study the dynamics of charge photogeneration in FSOCA on the picosecond timescale. First, a typical colloidal FSOCA sample was excited using a 360 nm pump pulse, and the TA spectrum was acquired with a broadband probe pulse (Fig. 4a). The spectrum exhibited a broad negative bleaching signal in the range of 450–520 nm assigned to the ground state bleach (GSB). In addition, the spectrum showed a broad positive signal from 540 to 700 nm (Fig. 4a). This positive signal could be attributed to trapped carriers (so-called "polarons" in FSOCA), because its formation was complementary to the decay of the GSB signal (Fig. 4a) [4,37-38].

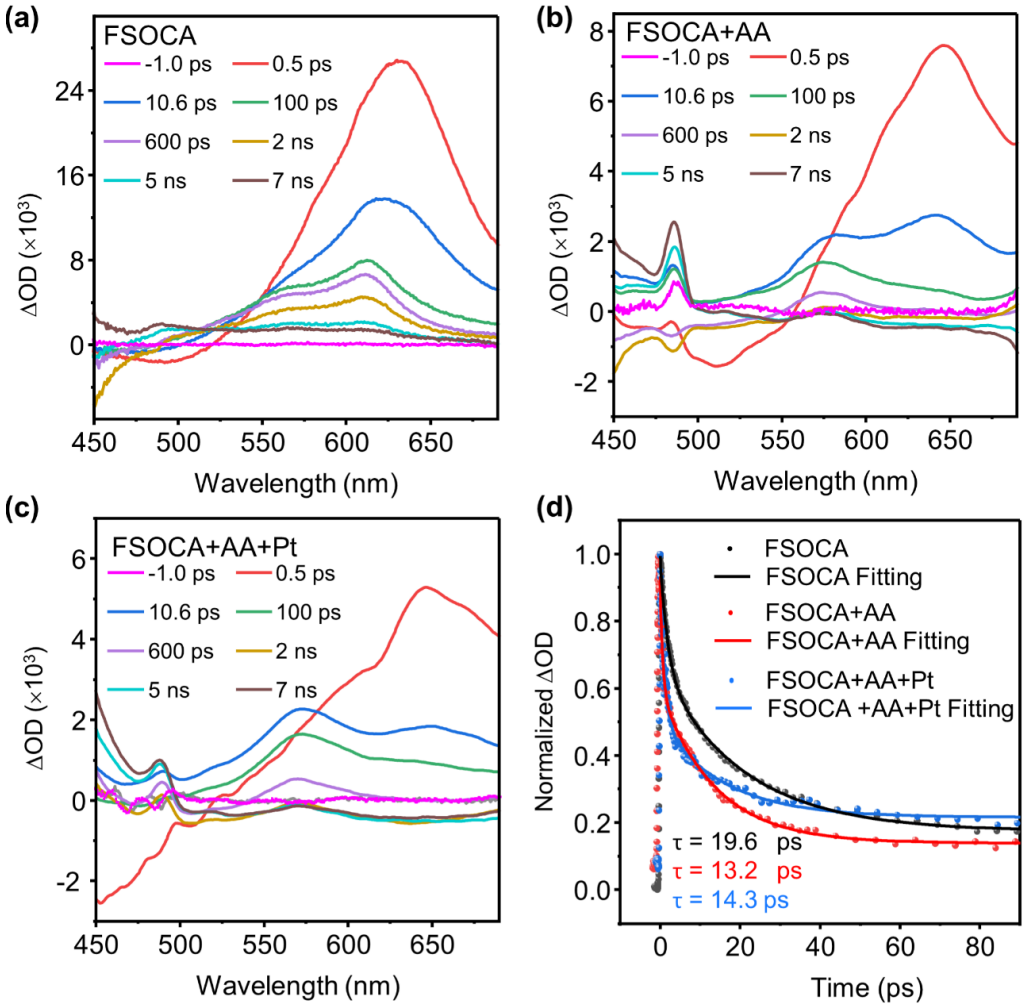

Figure 4. Transient absorption spectra obtained from suspensions of (a) FSOCA; (b) FSOCA + AA; (c) FSOCA + AA + Pt; (d) Comparison of transient absorption decay kinetics for FSOCA, FSOCA+AA and FSOCA+AA+Pt excited at 360 nm and probed at 650 nm.

The trapped carriers could be further assigned specifically as trapped holes on the basis of their rapid decay in the presence of the hole scavenger AA and AA + Pt. As shown in Supplementary Fig. 35, these trapped holes were transferred to AA for the significant decrease in signal intensity at 650 nm with the presence of AA and AA + Pt. The lifetime of charge carriers was studied by TA kinetics. As shown in Fig. 4d, the decay curves for the trapped hole of FSOCA, FSOCA + AA, and FSOCA + AA + Pt revealed quite different lifetimes (Supplementary Table 6). The lifetime of FSOCA + AA (13.2 ps) and FSOCA + AA + Pt (14.3 ps) were shorter than that of FSOCA (19.6 ps). These results further confirmed that the trapped holes were transferred to AA. Thus, it is clear that the introduction of AA captures the holes of FSOCA in several ps time scale, which decreases the probability of electron-hole recombination endow FSOCA a high activity for HER.

The interaction between FSOCA and AA

The interaction between sacrificial agents and catalysts in HER is also important for the overall electron transfer process. To get a better understanding of the impact of sulfone group on the interaction between FSOCA and AA, in situ attenuated total reflection surface-enhanced infrared absorption spectroscopy (ATR-SEIRAS) was utilized to monitor the adsorbed species near the electrochemical interface (Fig. 5a-5b). Using FSOCA and support as the electrochemical interfaces, background correction were carried out to avoid the interference of the signal of FSOCA and substrate before testing. The positive peak at 1758 cm^{-1} is attributed to the C═O stretching mode in the ester group of AA (Fig. 5a). In contrast, the C=O stretching mode in ester group of AA using TPCA as the electrochemical interfaces was observed at 1753 cm^{-1} (Fig. 5b). Furthermore, it was noted that the position of the C═O stretching mode did not shift with the change of applied potential for FSOCA and TPCA (Fig. 5c inset). While, the intensity of the band increases with decreasing potential for FSOCA, the intensity of the C═O stretching mode changes little with decreasing potential for TPCA (Fig. 5c) indicating that AA is specifically adsorbed to the FSOCA, but not on the TPCA [39]. Taken together, the ATR-SEIRAS results reveal that the interaction between FSOCA and AA is much stronger than that between TPCA and AA, which is likely due to hydrogen bond between the sulfone group and AA.

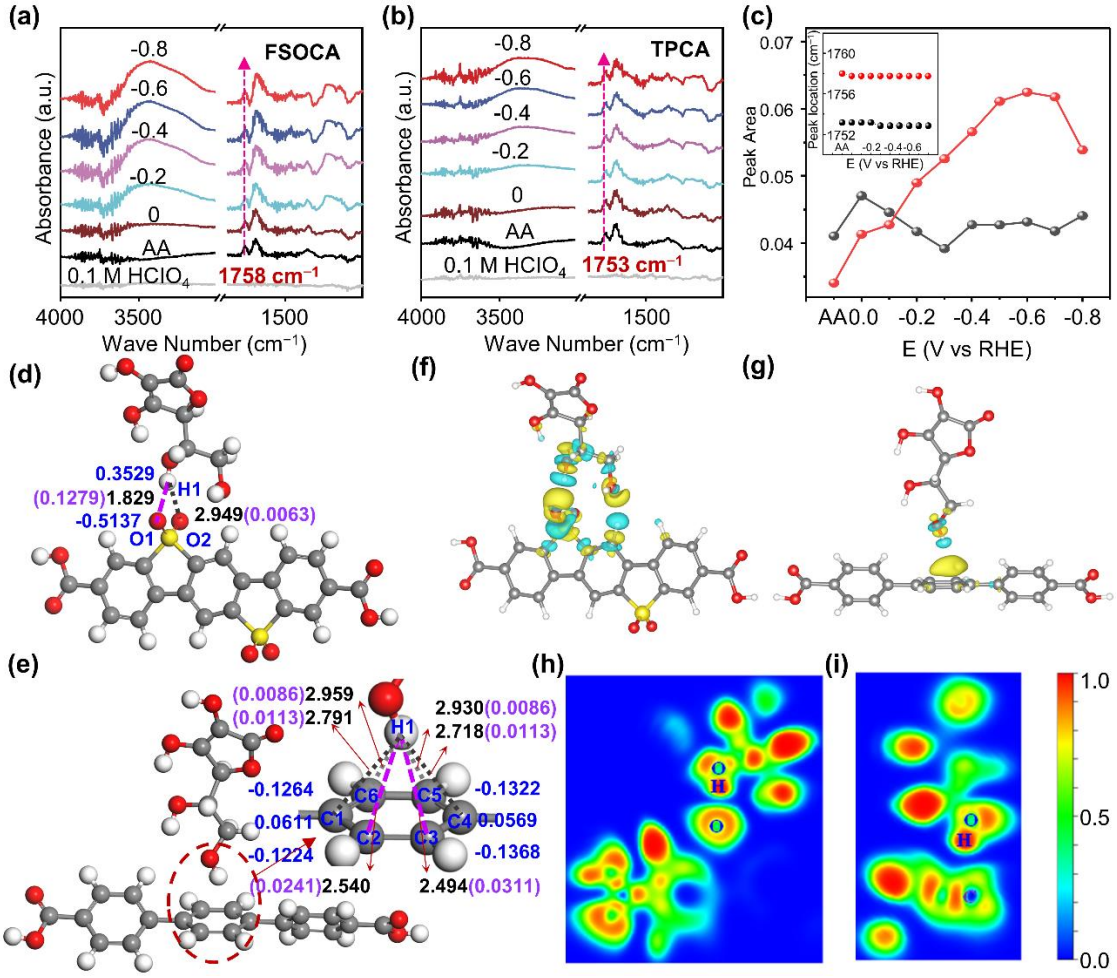

Figure 5. The SEIRA spectra and the DFT calculation. SEIRA spectra of (a) FSOCA; (b) TPCA; (c) The C=O peak area of AA on FSOCA and TPCA with the change of potential; the inset is the C=O peak of AA on FSOCA and TPCA. (d) Computation of the bond length (black), NACs (blue) and bond orders (purple) of AA adsorbed on FSOCA and (e) TPDA. Atoms are colored by element: H (white), C (gray), O (red), S (yellow). (f) Difference charge densities of AA adsorbed on FSOCA and (g) TPCA with an isosurface value of 0.001 e Bohr^{-3}, and the charge accumulation and depletion regions are colored in yellow and cyan. (h) Slab cut along O1-H1O and C3-H1O of ELF for AA adsorbed on FSOCA and (i) TPCA.

The interaction between AA and carboxyl acids (FSOCA and TPCA) were estimated by the theoretical calculation for quantification. The computed bond lengths of O1-H1 and O2-H1 were 1.829 and 2.949 Å of AA adsorbed on FSOCA, suggesting that AA tends to adsorb on the side of O atom, rather than between two O atoms (Fig.5d). The shortest bond lengths of C3-H1 and C2-H1 were 2.494 and 2.540 Å of AA adsorbed on TPCA (Fig.5e). It indicates that hydrogen bonds are formed between the hydroxyl groups in AA and the sulfonyl groups in FSOCA. The adsorption energies of AA on FSOCA and TPCA were found to be -0.40 and -0.19 eV, respectively. This means that the interaction of AA and FSOCA is stronger than that of AA and TPCA.

The charge density difference diagram clearly shows that the charge depletion regions on H1 atom of AA-FSOCA (Fig.5f) are larger than that of AA-TPCA (Fig.5g). Moreover, the blue regions between O1 and H1 atoms of AA-FSOCA are fewer than those of C3 and H1 atoms in AA-TPCA, as a whole, electron localization function (ELF) value is relatively small (Fig.5h, 5i). The density derived electrostatic and chemical (DDEC6) method is well-suited for studying materials containing hydrogen bonds. A quantitative atomic population analysis reveals that the hydrogen bond orders of the adsorption position in two materials are 0.1279 (Fig.5d, O1-H1) and 0.0241-0.0311 (Fig.5e, C2-H1, C3-H1), and the larger the O1-H1 (C3-H1) bond order, the higher AA molecule desorption energy becomes. The net atomic charges (NACs) of H atom are 0.3529 and 0.3293 |e|. The bond orders and NACs provide evidence for the difference in charge density and electron localization function diagram. These results show the hydrogen bonds have a significant electrostatic character and a smaller covalent character. To sum up, AA is more easily adsorbed and more stable on FSOCA rather than TPCA.

Conclusions

A rational design of a carboxyl acid groups bearing organic photocatalysts functionalized with sulfonyl groups (FSOCA) is reported that offers the necessary chemistry for photocatalytic hydrogen evolution reaction. The introduction of sulfonyl group can help to enhance the planarity and the hydrophilicity of FSOCA. The resulting materials FSOCA show efficient hydrogen evolution with a rate of 76

mmol g^{-1} h^{-1} ($\lambda > 320$ nm), which can stably produce hydrogen for at least 400 hours. The in situ attenuated total reflection surface-enhanced infrared absorption spectroscopy and computational calculation were utilized to explore the interaction between FSOCA and sacrificial agent, which suggests that AA is more easily adsorbed and more stable on FSOCA rather than unfunctionalized TPCA. These concepts may also be feasible for the design and synthesis of other organic photocatalysts. More importantly, because of the merits of FSOCA, such as its high activity, photocatalytic stability, solvent processibility and low-cost, make it a promising candidate to develop an efficient photocatalytic or photoelectrocatalytic system to achieve more complicated and challenging reactions, for example overall water splitting.

ASSOCIATED CONTENT

Supporting Information.
Experimental Methods section and SEM, TEM, FTIR, NMR, DLS analysis data. This material is available free of charge via the Internet at http://pubs.acs.org."

AUTHOR INFORMATION

Corresponding Author

* **Xiaoyan Wang**; Email: xiaoyan_wang@hust.edu.cn;
* **Bien Tan**; Email: bien.tan@mail.hust.edu.cn;

Author Contributions

X.W. and B. T. conceived the project. X. H. synthesized the materials, performed the characterization and photocatalysis experiments. X. Y. and X. Y carried out ATR-SEIRAS test and the data analysis. B. S. and L. Y. carried out the DFT calculation and interpreted the data. Z. Z. helped for the HRTEM test and analysis. R. S. and Y. G. helped for characterization. C. Z. helped with the writing. X. W. co-supervised with B. T., the work on molecules synthesis, characterization and photocatalysis. All authors interpreted the data and contributed to preparation of the manuscript.

Notes

The authors declare no competing financial interest.

ACKNOWLEDGMENT

This work was supported by the National Natural Science Foundation of China (Grant Nos. 21975086; Grant Nos. 52203259), the International S&T Cooperation Program of China (Grant No. 22161142005, 2018YFE0117300), Natural Science Foundation of Hubei Province (Grant No. 2022CFB720). X.Y. and X.Y. acknowledge the support from the HUST Academic Frontier Youth Team grant (Grant No. 2019QYTD11). We greatly appreciate the assistance of associate Prof. Songhua Cai from the Hong Kong Polytechnic University in conducting transmission electron microscope testing and analysis. And greatly appreciate the assistance of Dr. Tu Sun from ShanghaiTech University for microED test. We thank the Analysis and Testing Center, Huazhong University of Science and Technology, for assistance in the characterization of materials. Y. B. S. and L. M. Y. gratefully acknowledge the support from the National Natural Science Foundation of China (22073033, 21873032, 21673087, 21903032), the startup fund (2006013118 and 3004013105) from the Huazhong University of Science and Technology, the Fundamental Research Funds for the Central Universities (2019kfyRCPY116), and the Innovation and Talent Recruitment Base of New Energy Chemistry and Device (B21003). Y. B. S. and L. M. Y. are grateful for computational resources from the computing cluster at the School of Chemistry and Chemical Engineering, Huazhong University of Science and Technology. The work was carried out at the LvLiang Cloud Computing Center of China, and the calculations were performed on TianHe-2. The computing work in this paper is supported by the Public Service Platform of High Performance Computing by Network and Computing Center of HUST.

REFERENCES

(1) Zhao, D., Wang, Y., Dong, C., Huang, Y., Chen, J., Xue, F., Shen, S., Guo, L. Boron-Doped Nitrogen-Deficient Carbon Nitride-Based Z-Scheme Heterostructures for Photocatalytic Overall Water Splitting, *Nat. Energy* **2021**, *6*, 388–397.
(2) Nishiyama, H., Yamada, T., Nakabayashi, M., Maehara, Y., Yamaguchi, M., Kuromiya, Y., Nagatsuma, Y., Tokudome, H., Akiyama, S., Watanabe, T., Narushima, R., Okunaka, S., Shibata, N., Takata, T., Hisatomi, T., Domen, K. Photocatalytic Solar Hydrogen Production from Water on a 100-m^2 Scale. *Nature* **2021**, *598* (7880), 304–307.
(3) Guo, Y., Zhou, Q., Nan, J., Shi, W., Cui, F., Zhu, Y. Perylenetetracarboxylic Acid Nanosheets with Internal Electric Fields and Anisotropic Charge Migration for Photocatalytic Hydrogen Evolution. *Nat. Commun.* **2022**, *13* (1), 2067.
(4) Li, C., Liu, J., Li, H., Wu, K., Wang, J., Yang, Q. Covalent Organic Frameworks with High Quantum Efficiency in Sacrificial Photocatalytic Hydrogen Evolution. *Nat. Commun.* **2022**, *13* (1), 2357.
(5) Lan, Z., Zhang, G., Chen, X., Zhang, Y., Zhang, K., Wang, X. Reducing the Exciton Binding Energy of Donor–Acceptor-Based Conjugated Polymers to Promote Charge-Induced Reactions. *Angew. Chem. Int. Ed.* **2019**, *58* (30), 10236–10240.
(6) Wang, X., Maeda, K., Thomas, A., Takanabe, K., Xin, G., Carlsson, J., Domen, K., Antonietti, M. A Metal-Free Polymeric Photocatalyst for Hydrogen Production from Water under Visible Light, *Nat. Mater.* **2009**, *8*, 76–80.
(7) Yanagida, S., Kabumoto, A., Mizumoto, K., Pac, C., Yoshino, K. Poly(p-Phenylene)-Catalysed Photoreduction of Water to Hydrogen. *Chem. Commun.* **1985**, *8*, 474–475.
(8) Sachs, M., Sprick, R., Pearce, D., Hillman, S., Monti, A., Guilbert, A., Brownbill, N., Dimitrov, S., Shi, X., Blanc, F., Zwijnenburg, M., Nelson, J., Durrant, J., Cooper, A. Understanding Structure-Activity Relationships in Linear Polymer Photocatalysts for hydrogen evolution. *Nat. Commun.* **2018**, *9*, 4968.
(9) Sprick, R., Jiang, J., Bonillo, B., Ren, S.; Ratvijitvech, T., Guiglion, P., Zwijnenburg, M., Adams, D., Cooper, A. Tunable Organic Photocatalysts for Visible-Light-Driven Hydrogen Evolution. *J. Am. Chem. Soc.* **2015**, *137* (9), 3265–3270.
(10) Yang, C., Ma, B. C., Zhang, L., Lin, S., Ghasimi, S., Landfester, K., Zhang, K. A. I., Wang, X. Molecular Engineering of Conjugated Polybenzothiadiazoles for Enhanced Hydrogen Production by Photosynthesis. *Angew. Chem. Int. Ed.* 2016, 55 (32), 9202–9206.
(11) Li, L., Cai, Z., Wu, Q., Lo, W.-Y., Zhang, N., Chen, L. X., Yu, L. Rational Design of Porous Conjugated Polymers and Roles of Residual Palladium for Photocatalytic Hydrogen Production. *J. Am. Chem. Soc.* **2016**, *138* (24), 7681–7686.
(12) Wang, X., Chen, L., Chong, S. Y., Little, M. A., Wu, Y., Zhu, W.-H., Clowes, R., Yan, Y., Zwijnenburg, M. A., Sprick, R. S., Cooper, A. I. Sulfone-Containing Covalent Organic Frameworks for Photocatalytic Hydrogen Evolution from Water. *Nat. Chem.* **2018**, *10* (12), 1180–1189.
(13) Wang, H., Wang, H., Wang, Z., Tang, L., Zeng, G., Xu, P., Chen, M., Xiong, T., Zhou, C., Li, X., Huang, D., Zhu, Y., Wang, Z., Tang, J. Covalent Organic Framework Photocatalysts: Structures and Applications. *Chem. Soc. Rev.* **2020**, *49* (12), 4135–4165.

(14) Wang, H., Zeng, Z., Xu, P., Li, L., Zeng, G., Xiao, R., Tang, Z., Huang, D., Tang, L., Lai, C., Jiang, D., Liu, Y., Yi, H., Qin, L., Ye, S., Ren, X., Tang, W. Recent Progress in Covalent Organic Framework Thin Films: Fabrications, Applications and Perspectives. *Chem. Soc. Rev.* **2019**, *48* (2), 488–516.
(15) Hu, X., Zhan, Z., Zhang, J., Hussain, I., Tan, B. Immobilized Covalent Triazine Frameworks Films as Effective Photocatalysts for Hydrogen Evolution Reaction. *Nat. Commun.* **2021**, *12* (1), 6596.
(16) Liu, M., Huang, Q., Wang, S., Li, Z., Li, B., Jin, S., Tan, B. Crystalline Covalent Triazine Frameworks by In Situ Oxidation of Alcohols to Aldehyde Monomers. *Angew. Chem. Int. Ed.* **2018**, *57* (37), 11968–11972.
(17) Wang, K., Yang, L. M., Wang, X., Guo, L., Cheng, G., Zhang, C., Jin, S., Tan, B., Cooper, A. Covalent Triazine Frameworks via a Low-Temperature Polycondensation Approach. *Angew. Chem. Int. Ed.* **2017**, *56* (45), 14149–14153.
(18) Sun, T., Liang, Y., Xu, Y. Rapid, Ordered Polymerization of Crystalline Semiconducting Covalent Triazine Frameworks. *Angew. Chem. Int. Ed.* **2022**, *61* (4), e202113926.
(19) Han, C., Xiang, S., Jin, S., Zhang, C., Jiang, J., Rational Design of Conjugated Microporous Polymer Photocatalysts with Definite D−π−A Structures for Ultrahigh Photocatalytic Hydrogen Evolution Activity under Natural Sunlight. *ACS Catal.* **2023**, *13* (1), 204–212.
(20) Lin, L., Lin, Z., Zhang, J., Cai, X., Lin, W., Yu, Z., Wang, X. Molecular-Level Insights on the Reactive Facet of Carbon Nitride Single Crystals Photocatalysing Overall Water Splitting. *Nat. Catal.* **2020**, *3* (8), 649–655.
(21) Algara, G., Severin, N., Chong, S. Y., Björkman, T., Palgrave, R. G., Laybourn, A., Antonietti, M., Khimyak, Y. Z., Krasheninnikov, A. V., Rabe, J. P., Kaiser, U., Cooper, A. I., Thomas, A., Bojdys, M. J. Triazine-Based Graphitic Carbon Nitride: A Two-Dimensional Semiconductor. *Angew. Chem. Int. Ed.* **2014**, *53* (29), 7450–7455.
(22) Lin, L., Wang, C., Ren, W., Ou, H., Zhang, Y., Wang, X. Photocatalytic Overall Water Splitting by Conjugated Semiconductors with Crystalline Poly(Triazine Imide) Frameworks. *Chem. Sci.* **2017**, *8* (8), 5506–5511.
(23) Aitchison, C. M., Kane, C. M., McMahon, D. P., Spackman, P. R., Pulido, A., Wang, X., Wilbraham, L., Chen, L., Clowes, R., Zwijnenburg, M. A., Sprick, R. S., Little, M. A., Day, G. M., Cooper, A. I. Photocatalytic Proton Reduction by a Computationally Identified, Molecular Hydrogen-Bonded Framework. *J. Mater. Chem. A* **2020**, *8* (15), 7158–7170.
(24) Zhu, Y., Zhang, Z., Si, W., Sun, Q., Cai, G., Li, Y., Jia, Y., Lu, X., Xu, W., Zhang, S., Lin, Y. Organic Photovoltaic Catalyst with Extended Exciton Diffusion for High-Performance Solar Hydrogen Evolution. *J. Am. Chem. Soc.* **2022**, *144* (28), 12747–12755.
(25) Zhang, Z., Si, W., Wu, B., Wang, W., Li, Y., Ma, W., Lin, Y. Two-Dimensional Polycyclic Photovoltaic Molecule with Low Trap Density for High-Performance Photocatalytic Hydrogen Evolution. *Angew. Chem. Int. Ed.* **2022**, *61* (10), e202114234.
(26) Weingarten, A. S., Kazantsev, R. V., Palmer, L. C., McClendon, M., Koltonow, A. R., Samuel, A. P. S., Kiebala, D. J., Wasielewski, M. R., Stupp, S. I. Self-Assembling Hydrogel Scaffolds for Photocatalytic Hydrogen Production. *Nat. Chem.* **2014**, *6* (11), 964–970.
(27) Dannenhoffer, A. J., Sai, H., Harutyunyan, B., Narayanan, A., Powers-Riggs, N. E., Edelbrock, A. N., Passarelli, J. V., Weigand, S. J., Wasielewski, M. R., Bedzyk, M. J., Palmer, L. C., Stupp, S. I. Growth of Extra-Large Chromophore Supramolecular Polymers for Enhanced Hydrogen Production. *Nano Lett.* **2021**, *21* (9), 3745–3752.
(28) Weingarten, A. S., Dannenhoffer, A. J., Kazantsev, R. V., Sai, H., Huang, D., Stupp, S. I. Chromophore Dipole Directs Morphology and Photocatalytic Hydrogen Generation. *J. Am. Chem. Soc.* **2018**, *140* (15), 4965–4968.
(29) Kong, K., Zhang, S., Chu, Y., Hu, Y., Yu, F., Ye, H., Ding, H., Hua, J. A Self-Assembled Perylene Diimide Nanobelt for Efficient Visible-Light-Driven Photocatalytic H_2 Evolution. *Chem. Commun.* **2019**, *55* (56), 8090–8093.
(30) Jing, J., Yang, J., Zhang, Z., Zhu, Y. Supramolecular Zinc Porphyrin Photocatalyst with Strong Reduction Ability and Robust Built-In Electric Field for Highly Efficient Hydrogen Production. *Adv. Energy Mater.* **2021**, *11* (29), 2101392.
(31) Zhang, N., Wang, L., Wang, H., Cao, R., Wang, J., Bai, F., Fan, H., Self-Assembled One-Dimensional Porphyrin Nanostructures with Enhanced Photocatalytic Hydrogen Generation. *Nano Lett.* **2018**, *18* (1), 560-566.
(32) Zhang, Z., Zhu, Y., Chen, X., Zhang, H., Wang, J. A Full-Spectrum Metal-Free Porphyrin Supramolecular Photocatalyst for Dual Functions of Highly Efficient Hydrogen and Oxygen Evolution. *Adv. Mater.* **2019**, *31* (7), 1806626.
(33) Zhang, G., Yang, X., Li, Y., Zhang, P., Mi, H. Donor–Acceptor Cyanocarbazole-Based Supramolecular Photocatalysts for Visible-Light-Driven H_2 Production. *ChemSusChem*, **2019**, *12* (23), 5070–5074.
(34) Yang, H., Li, C., Liu, T., Fellowes, T., Chong, S. Y., Catalano, L., Bahri, M., Zhang, W., Xu, Y., Liu, L., Zhao, W., Gardner, A., Clowes, R., Browning, N., Li, X., Cowan, A., Cooper, A. Packing-Induced Selectivity Switching in Molecular Nanoparticle Photocatalysts for Hydrogen and Hydrogen Peroxide Production. *Nat. Nanotechnol.* **2023**, *18* (3), 307–315.
(35) Liang, Y., Li, T., Lee, Y., Zhang, Z., Li, Y., Si, W., Liu, Z., Zhang, C., Qiao, Y., Bai, S., Lin, Y. Organic Photovoltaic Catalyst with σ-π Anchor for High-Performance Solar Hydrogen Evolution. *Angew. Chem. Int. Ed.* **2023**, *62* (12), e202217989.
(36) Hillman S. A. J., Sprick R. S., Pearce D., Woods D. J., Sit W-Y., Shi X. Y., Cooper A. I., Durrant J. R., Nelson J., *J. Am. Chem. Soc.* **2022**, *144* (42), 19382-19395
(37) Clarke, T. M., Durrant, J. R. Charge Photogeneration in Organic Solar Cells. *Chem. Rev.* **2010**, *110* (11), 6736–6767.
(38) Kosco, J., Gonzalez-Carrero, S., Howells, C. T., Fei, T., Dong, Y., Sougrat, R., Harrison, G. T., Firdaus, Y., Sheelamanthula, R., Purushothaman, B., Moruzzi, F., Xu, W., Zhao, L., Basu, A., De Wolf, S., Anthopoulos, T. D., Durrant, J. R., McCulloch, I. Generation of Long-Lived Charges in Organic Semiconductor Heterojunction Nanoparticles for Efficient Photocatalytic Hydrogen Evolution. *Nat. Energy*, **2022**, *7*, 1–12.
(39) Yang, X., Nash, J., Oliveira, N., Yan, Y., Xu, B. Understanding the PH Dependence of Underpotential Deposited Hydrogen on Platinum. *Angew. Chem. Int. Ed.* **2019**, *58* (49), 17718–17723.

SYNOPSIS TOC

We report here a sulfone-functionalized molecular single crystal that integrates the necessary chemistry (low exciton binding energy, hydrophilic, high crystalline) for efficient photocatalytic hydrogen evolution.